J Mater Sci: Mater Electron (2021) 32:13418–13429

Fabrication of dye-sensitized solar cells with ZnO nanorods as photoanode and natural dye extract as sensitizer

P. Dhamodharan[1,2], Jian Chen[1,*], and C. Manoharan[2,*]

[1] *Jiangsu Key Laboratory of Advanced Metallic Materials, School of Materials Science and Engineering, Southeast University, Nanjing 211189, Jiangsu, People's Republic of China*

[2] *Department of Physics, Annamalai University, Annamalai Nagar, Chidambaram 608002, Tamil Nadu, India*

Received: 2 December 2020
Accepted: 4 April 2021
Published online: 30 April 2021

ABSTRACT

Highly oriented zinc oxide nanorods (ZnO NRs) have been grown on ITO substrates at various growth times using hydrothermal method. The necessary ZnO seed layers on ITO have been deposited using spray pyrolysis. Both the methods have been successfully applied to prepare efficient ZnO NRs-based photoanodes for DSSCs. FESEM images revealed the vertical growth of ZnO NRs from the substrates with a length and diameter ranges of 1.2–1.5 μm and 80–120 nm, respectively. The XRD and HRTEM results confirmed the hexagonal structure with preferential orientation (c-axis) of ZnO NRs. The high optical transmittance (90%) was observed in the visible region for the ZnO NRs grown for 9 h. A decrease in optical bandgap was noticed with the increase of growth times. The natural dye extract absorbed in to the ZnO NRs exhibited a broad absorption peak in UV–Vis spectra analysis. The power conversion efficiency of DSSCs prepared with ZnO NRs (9 h) as photoanode showed better performance compared to other growth times.

1 Introduction

Energy is an essential feature of the development of humankind. Extensive research has been a wide investigation on the development of clean renewable energy resources to reduce energy demands and environmental pollution [1]. Among the different renewable energy sources, solar energy is the basic source because of its low environmental pollution and worldwide availability. In 1990, Gratzel et al. has developed a novel type of solar cell, known as dye-sensitized solar cells (DSSCs) or Grätzel cell [2]. The fabrication of DSSCs based on low-cost technologies have given the scope for its promising applications in harvesting solar energy with higher power conversion efficiency (PCE) than other solar cells [3–5].

Zinc oxide is one of the oldest earth abundant semiconductor oxide materials widely researched in different fields, as it is nontoxic, wide bandgap, flexible multifunctional material [6]. Also, as it

Address correspondence to E-mail: j.chen@seu.edu.cn; cmanoharan1@rediffmail.com

https://doi.org/10.1007/s10854-021-05920-8

possesses good chemical and photostability, high exciton binding energy, high carrier conductivity and mobility, good transparency, tunable bandgap, high piezoelectric effect and high refractive index, it is used in different fields, such as gas sensor, LEDs, cosmetics, photocatalyts, solar cells, piezoelectric, varistor, and optoelectronic devices [7–14]. Over the past few decades, ZnO nanostructures has been considered as one of the best alternative electrode materials for the most widely used TiO_2 because of their similar properties [15]. The PCE of the DSSCs depends on the morphology of the photoanode. The photoanode must possess good charge separation, high charge collection, high electron mobility, large surface area, and high light scattering ability [16]. Recent survey revealed that many researchers have prepared various ZnO-based nano-structured (nanoparticles, nanorods, nanowires, nanoribbon, nanowalls, nanofiber, and nanoneedle) electrode materials to improve the photovoltaic performance of solar cells [17]. Among these structures, ZnO nanoparticles used as photoanode in DSSCs with larger surface area have slower electron transfer, which is attributed to the multi-trapping events.

To solve these issues, one-dimensional (1D) ZnO NRs were considered, which considerably enhanced the electron transfer in photoanodes for DSSCs cell and photoanodes rapidly stored photovoltaic electrons via the direct conduction path provided by the photons. Hence, 1D ZnO NRs, which not only improve the electron transport but also increase light absorption and decreases the electron diffusion distance, thereby reduce the charge recombination. ZnO nanorod arrays not only increase surface area but also promote an enhanced charge transport property due to the improvement of direct electron conduction when compared with scattered ZnO nanoparticles [18].

Many methods, like chemical vapor deposition, MOCVD, pulsed laser deposition, and hydrothermal and thermal evaporation, are devoted for preparing nanorods depending on the field of application [19–23]. However, ZnO NRs prepared by hydrothermal method is broadly used as a photoanode in DSSCs because of cost-effectiveness, less hazardous, simplicity in the mechanism, easy adaptability, eco-friendly, and large-scale production for commercialization [24]. Generally, pre-coated glass plates are used in the hydrothermal method to achieve growth direction and to control morphology of ZnO NRs [25].

Several deposition techniques were employed to prepare the seeded substrates that are metal organic chemical vapor deposition (MOCVD) [26], sputtering [27], sol–gel [28], and spray pyrolysis [29]. Among these, the spray pyrolysis technique becomes a significant one in recent years, as the basic structural and morphological characteristics of the prepared materials can be controlled by growth conditions with which the grown film leading to exhibit the essential functionality for particular applications [30]. Yuanyao Dou et al. deposited Ga-doped ZnO seed layer on FTO substrate by using sol–gel followed by hydrothermal method and they obtained ZnO nanorods. A decrease in diameter and density of the ZnO nanorods with enhanced DSSCs performance was noticed with increasing Ga concentration [31].

In this present work is to optimize the parameters to grow ZnO NRs using hydrothermal method and to investigate the performance of grown ZnO NRs on ITO substrates as photoanode in DSSCs. The structural, optical, and electrical properties of prepared ZnO NRs were analyzed. The surface morphology (length and diameter) of ZnO NRs was carefully controlled by adjusting the growth times at a hydrothermal temperature to improve the carrier mobility and concentration. Finally, the photovoltaic performance was examined by the efficiency of the fabricated DSSCs.

2 Experimental part

2.1 Preparation of ZnO seed layer

The ZnO thin films were deposited onto ITO substrates by spray pyrolysis technique. Standard spray pyrolysis procedure was reported in “Elsevier” [32]. 0.1 M of $ZnC_{10}H_{14}O_5$ precursor was dissolved in ethanol and the solution was sprayed onto the ITO substrates maintained at 350 °C for 15 min. During the spray process the spray rate and substrate to nozzle distance were 3 ml/min and 23 cm, respectively. The prepared films are allowed to cool slowly to room temperature, which is the seed layer for the growth of ZnO NRs by hydrothermal method.

2.2 Growth of well-aligned ZnO NRs

The ZnO seed layer coated ITO substrate using spray technique was kept upside-down in the conventional beaker with aqueous solution (100 ml) containing 0.02 mol of zinc acetate and 0.4 mol of sodium hydroxide. Then the beaker was kept in the autoclave and nanorods were grown at a temperature of 95 °C for different growth times. After the growth, the substrates were rinsed with deionized water and ethanol and dried in air. Further, the samples were annealed at 400 °C for 1 h in muffle furnace. The films grown for 3 h, 6 h and 9 h were named as ZnO NRs 3 h, 6 h, and 9 h, respectively (Fig. 1a).

2.3 Dye extraction

Natural dye extracts are prepared using the following procedure: 10 g of fresh flower petals (*hibiscus rosa-sinensis)* were cut into small pieces and kept in a beaker. The chopped petals were soaked in 50 ml ethanol by using an indirect hydronic heating method in boiling water and refluxed for 15–30 min. Finally, the solid dregs were filtered out by using filter paper and the obtained pure natural dye solution was stored properly. To investigate the effect of solvents on the performance of DSSCs, dye extract of *hibiscus rosa-sinensis* were prepared using various solvents, such as, ethanol, water, and methanol. The schematic diagram of dye extract preparation is depicted in Sect. 3.5.

2.4 Preparation of electrolyte

The electrolyte is an essential part of DSSCs and its function is collecting the charge carriers at the cathode and return the electrons to the dye molecules. In organic solvents, I^-/I^{3-} is commonly used as the electrolyte in acetonitrile solution. Lithium ion (Li) was included in this work to ensure that electron transport takes place without interruption. The electrolyte is prepared using the combination of 0.3 M of Lithium Iodide (LiI) and 0.03 M of Iodine (I_2) in acetonitrile and tert-butyl alcohol.

2.5 Working principles of DSSCs

DSSCs consist two transparent conducting electrodes in a sandwich arrangement (Fig. 1b). Each layer has a specific function in the cell. The transparent electrodes allow the absorbed sunlight to dye molecule layer. The nanocrystalline semiconductor (ZnO NRs) provides an important surface area for dye absorption. The dye molecules which absorb photon from sunlight are excited to LUMO from the HOMO. The dye molecules become oxidized after the injection of the electron into the conduction band of nanoporous semiconductor (ZnO NRs).

This introduced electrons are transported through the nanoporous semiconductor thin film toward the conductive electrode (anode). Finally, the electron travels through the wire (external load) and reaches the counter electrode (cathode) after performing the work, as electrical energy. The electrons reaching the cathode are transferred to the electrolyte. The electrolytes (I/I_3) act as a connecter between cathode and ZnO NR photoanodes. The Iodide ion (I) on redox releases the electron, which replaces the electron lost by the dye molecule. On redox, (I^-) becomes I^{3-} and is regenerated to I^- by receiving an electron from the counter electrode. The circuit is fulfilled by the foreign electron through the external load.

2.6 Characterization techniques

The crystallographic properties of ZnO NRs were analyzed through a SHIMADZU-6000 X-ray diffractometer. The morphology was determined from a SUPRA 55 Carl Zeiss using field emission scanning electron microscopy (FESEM) attached with EDS. Optical measurements were studied using the JASCO V-670 spectrophotometer and PL analysis of the nanorods was recorded using 450 W Xenon lamp as the excitation source with VARIAN spectrophotometer. The electrical properties were carried out by Hall Effect measurement system (ECOPIA HMS-3000) in van der Pauw's configuration. The current–voltage tests were examined by using a Keithley (2450 source meter) under the illumination of the simulated at standard test condition (100 mW cm^{-2}, AM 1.5G).

3 Results and discussion

3.1 Surface morphology and compositional analysis

Figure 2 shows the surface morphologies of the ZnO NRs at various growth times. Figure 2a, b, d, and e

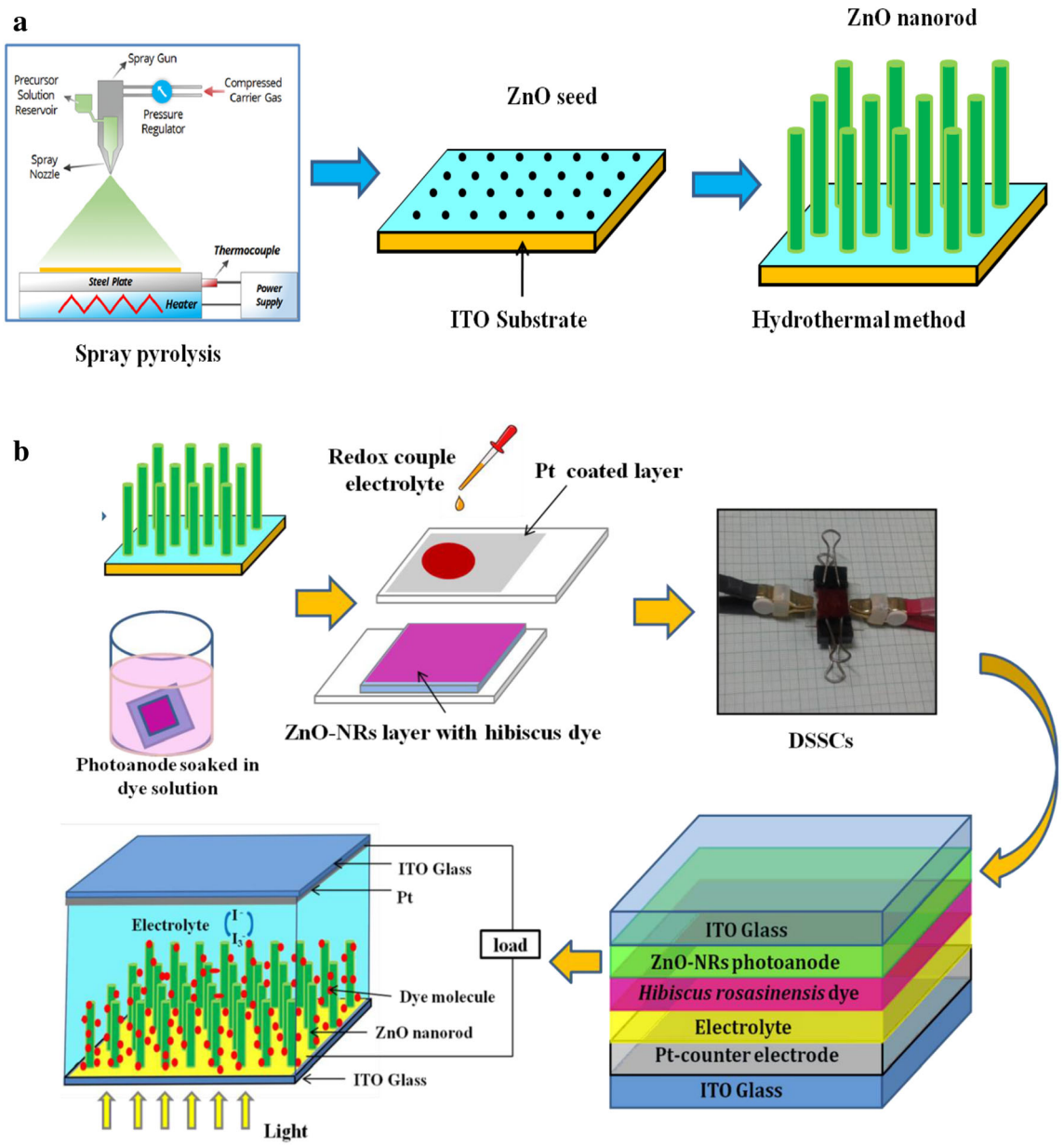

Fig. 1 **a** Schematic diagram for preparation of ZnO NRs. **b** Working principle of ZnO NRs based DSSCs

shows uniformly distributed ZnO NRs (3 and 6 h) covered the entire surface with the hexagonal shape on the top surface to confirm the stable structure. On increasing the growth time, the density of ZnO NRs (9 h) is being increased (Fig. 2g–h). The hexagonal-shaped ZnO NRs with the large surface area can improve the dye absorption for dye-sensitized solar cells and are expected to provide promising industrial photocatalytic applications. Vertically well-aligned ZnO NRs grown from the substrates have uniform thickness and length distribution. The length and diameter of NRs are in the ranges 1.2–1.5 μm and 80–120 nm, respectively. The cross-sectional images indicate that ZnO NRs (length and diameter) can be controlled by adjusting the growth time. Figure 2c, f, and i illustrates the cross-sectional images of ZnO NRs, which corresponds to the growth time at 3, 6, and 9 h, respectively. Energy dispersive X-ray spectroscopy (EDS) was used to identify the type of elements present in the samples. The EDS spectrum of ZnO NRs (9 h) exhibited the distinguished peaks of elements Zn and O (Fig. 3). The atomic percentage ratio of Zinc (51.76) and Oxygen (48.24) is nearly close to stoichiometric ZnO. Both the elements Zinc

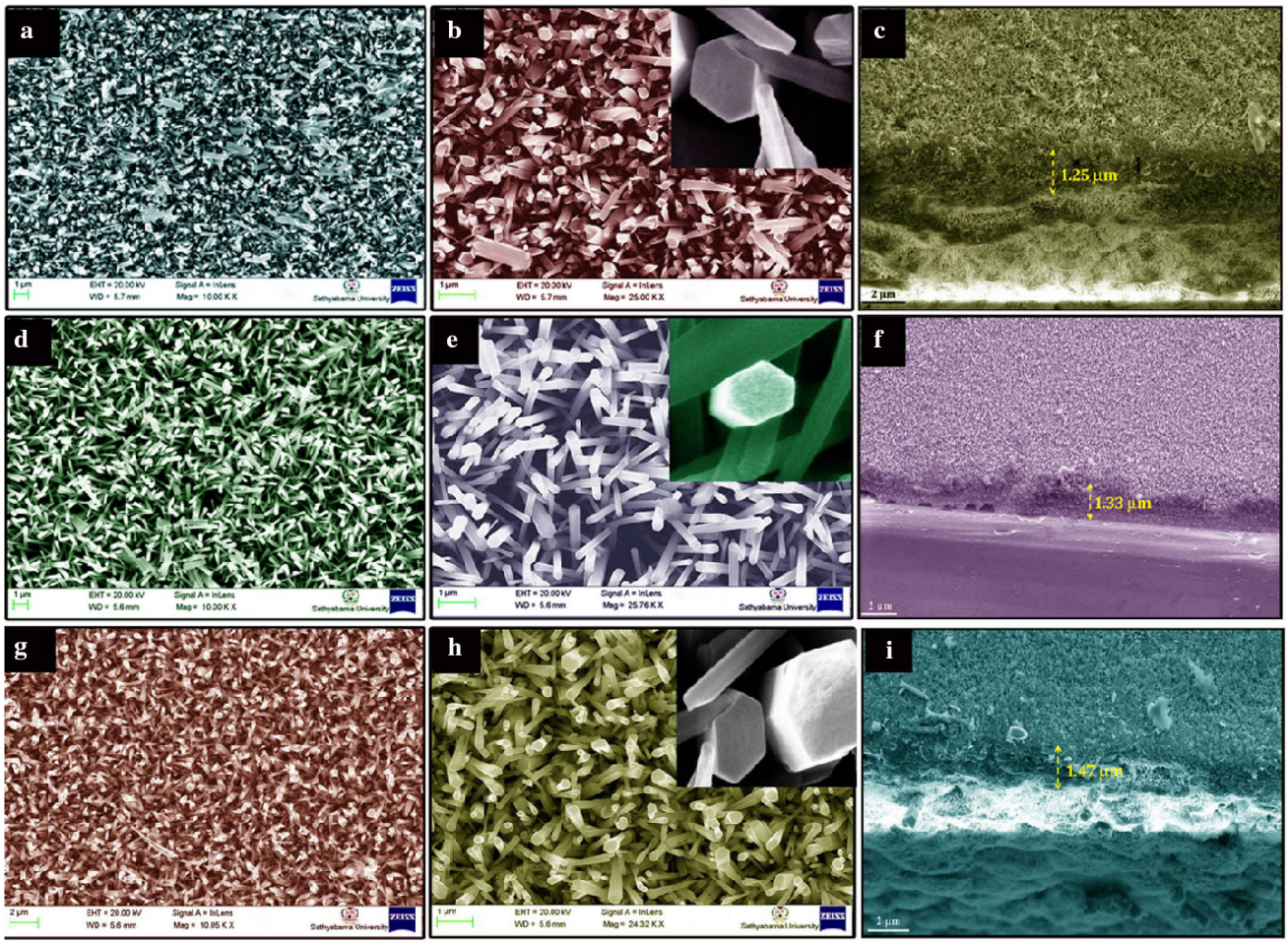

Fig. 2 FESEM images of ZnO NRs with different growth times **a**, **b** 3 h, **d**, **e** 6 h, **g**, **h** 9 h, **c**, **f** and **i** Corresponding cross-sectional images

and oxygen together contribute 100% of the total weight. This result indicates that the prepared samples are pure ZnO and free from impurities [33].

3.2 Structural analysis

The crystallographic properties of prepared ZnO NRs are determined by the XRD pattern. Figure 4 represents the XRD pattern of ZnO NRs at different hydrothermal growth times.

The observed diffraction peaks are perfectly indexed to the hexagonal crystal structure of ZnO and calculated lattice constant values, a = 3.245, c = 5.206, and space group = P63mc, which are in well consistent with standard JCPDS card no 36–1451. The diffraction patterns with 2θ values 34.50°, 36.52°, 47.58°, 56.82°, 63.05°, 66.68°, and 69.40° are corresponding to the planes (002), (101), (102), (110), (103), (200), and (201) of ZnO NRs, respectively [33]. No other secondary peaks (related to Zn or ZnO_2) have been detected in the XRD pattern. On increasing the hydrothermal growth time from 3 to 9 h, the observed sharp and intense peak in XRD pattern revealed better crystallinity and preferential orientation (002) along c-axis that is normal to substrate surface. Kahraman et al. [34] reported that the greater intensity of (002) plane indicates the preferential orientation of crystallites along the c-axis normal to the substrate.

The trend to lower the surface energy during growth is the reason for the self-ordering effect and hence preferential orientation takes place [34]. The average crystallite size is calculated using Debye–Scherer formula [35], and the values are given in Table 1. The increase of crystallite size with increasing growth times shows the enhancement of crystallinity.

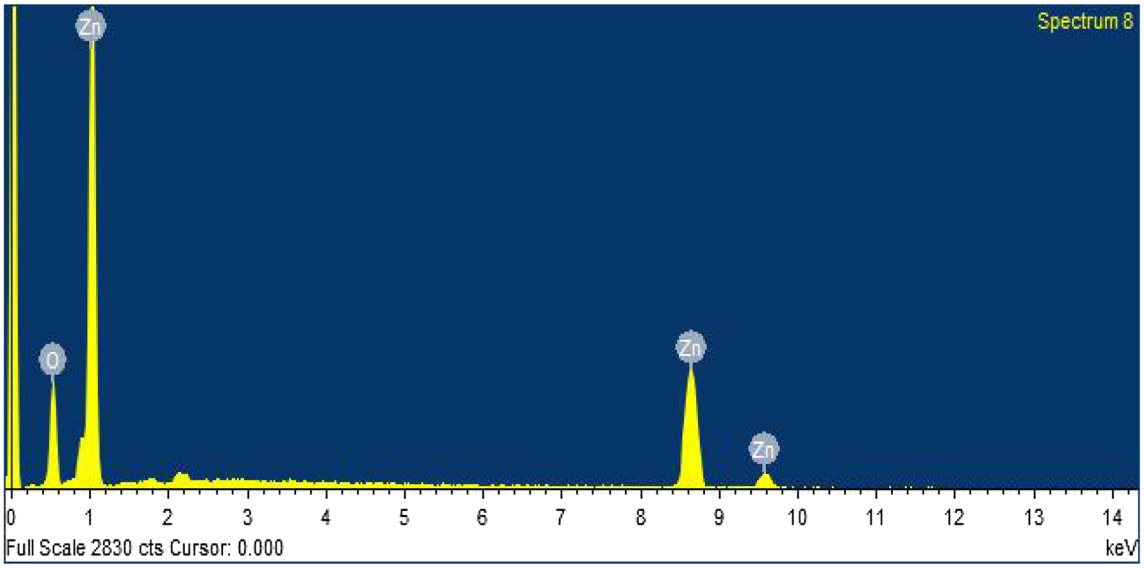

Fig. 3 EDS spectrum of ZnO NRs

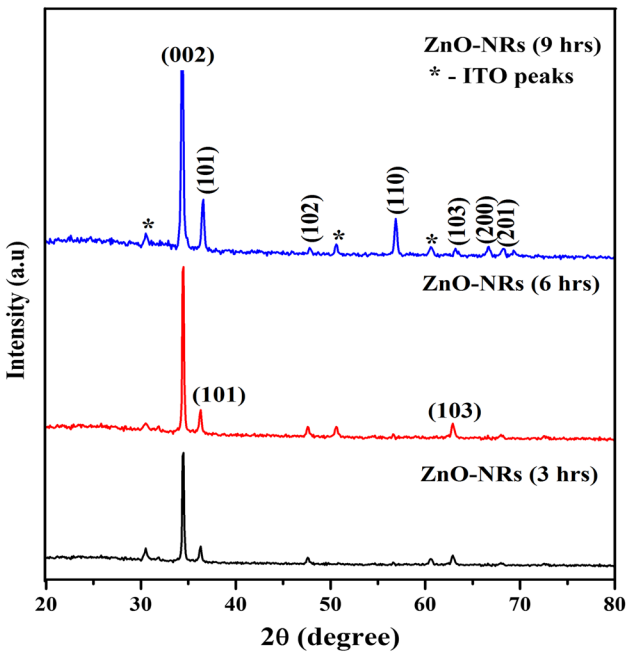

Fig. 4 XRD pattern of ZnO NRs with various growth times

3.3 HRTEM analysis

HRTEM and SAED patterns are also used to analyze the microstructure of ZnO NRs prepared with growth time of 9 h. Figure 5a shows the lattice fringe spacing value of 0.26 nm, which is in good agreement with the inter-planer spacing of the (002) planes of the hexagonal ZnO. These findings confirm once again the structure of nanorods exhibiting preferential c-axis orientation. The TEM micrograph of the prepared sample shows rod-like morphology (inset Fig. 5a). The SAED patterns shown in Fig. 5b reveal the presence of sporty diffraction rings with regular spot patterns, which confirms the crystalline nature with growth along the c-axis direction.

3.4 Optical properties

Figure 6 shows the optical absorption spectrum of ZnO NRs with different growth times.It was found that the optical absorption edge value of ZnO NRs is 380, 384, and 390 nm for the growth times 3, 6, and 9 h, respectively. The transmittance spectra of ZnO NRs at various growth times are depicted in Fig. 7. The nanorods are highly transparent in the visible region and transmittance values increase with the increase of growth time. The higher transmittance value of ZnO NRs with growth time 9 h is associated with better crystalline quality and a higher ratio of length/diameter. The highest ratio of length/diameter of ZnO NRs is the essential parameter for increased light trapping in solar cells [36]. The obtained results are consistent with the observed FESEM results.

The optical bandgap is another important optical parameter of the TCO materials, which is used for photovoltaic applications. The bandgap of ZnO nanorods was obtained by extrapolating the linear part of the plots of $(\alpha h\upsilon)^2$ verses $h\upsilon$. Figure 8 shows the optical bandgap (E_g) values of 3.26, 3.23, and 3.18 eV for the ZnO NRs grown for 3, 6, and 9 h,

Table 1 The structural and electrical properties ZnO nanorods prepared at various growth times

Samples (Hours)	h k l plane	Crystallite Size (D) nm	Resistivity ρ (Ω cm) × 10^{-4}	Carrier concentration n (cm^{-3}) × 10^{21}	Mobility μ (cm^2/Vs)
3	002	33	1.24	15.50	32.52
6	002	35	1.12	16.12	34.65
9	002	38	0.75	21.22	39.28

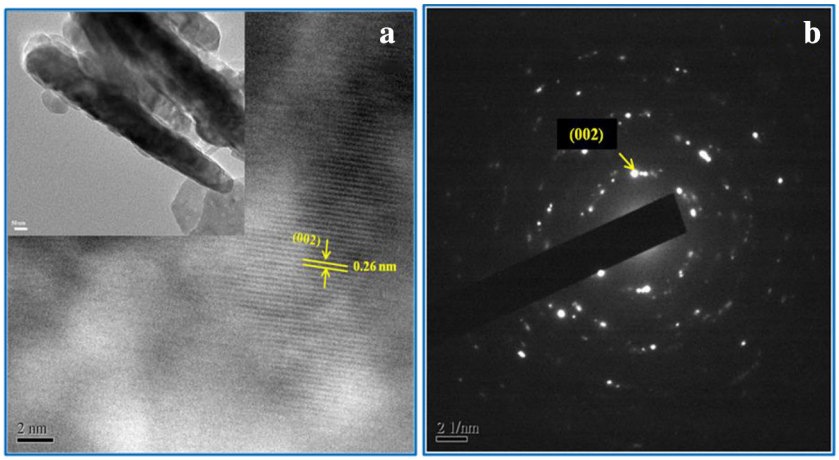

Fig. 5 TEM analysis of ZnO NRs **a** Fringe pattern (Inset Fig. Images), **b** SAED Pattern

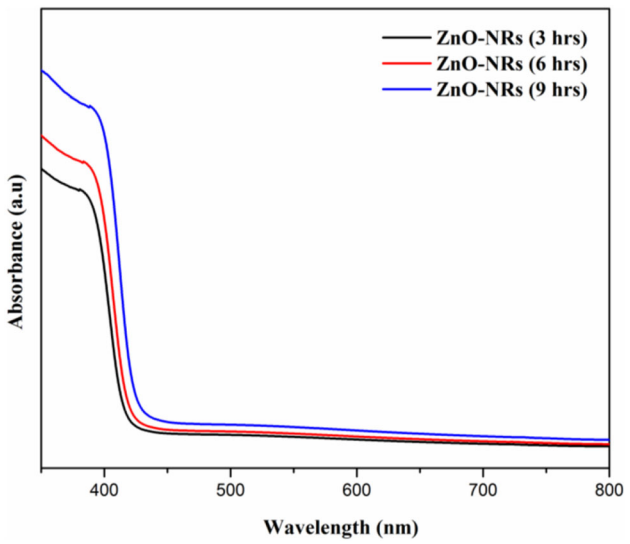

Fig. 6 UV–Visible absorption spectra of ZnO NRs prepared at various growth times

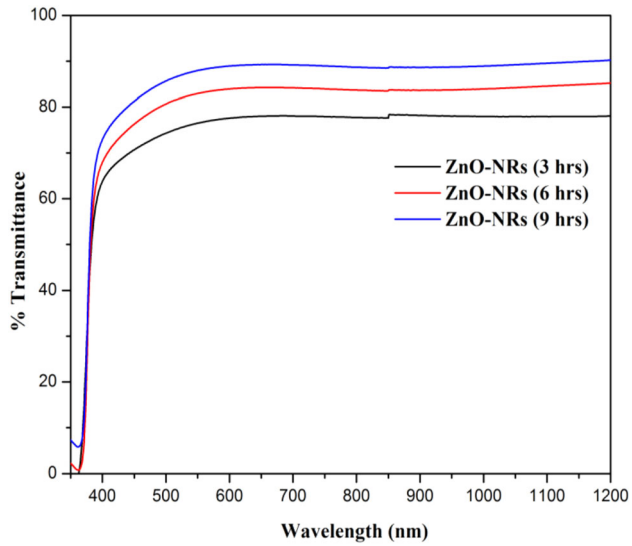

Fig. 7 Transmittance spectra of ZnO NRs prepared at various growth times

respectively. A decrease in optical bandgap is noticed with the increase of growth time, which is due to the quantization effect of photo-generated electron–hole pairs. The tunable bandgap with growth time contributes to enhance the efficiency of DSSCs.

3.5 Photoluminescence

Photoluminescence analysis allows the investigation of electronic structure and optical features of semiconducting materials by generating information on defects, surface oxygen vacancies, along with separation, and recombination of photoinduced charge

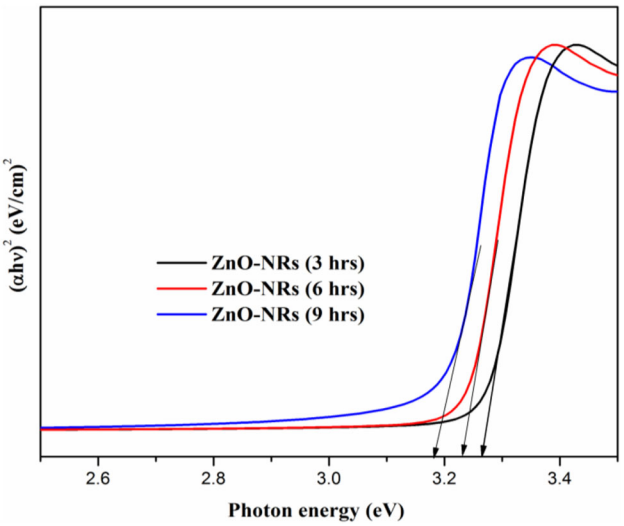

Fig. 8 Plots of $(\alpha h\upsilon)^2$ vs $(h\upsilon)$ for ZnO NRs prepared at various growth times

carriers [37]. The room temperature photoluminescence (PL) spectra of nanorods are shown in Fig. 9. ZnO NRs exhibit intense UV emission located at 395 nm and one more deep-level emission at 515 nm. The greater intensity of NBE emission originates from ZnO NRs reveals a good crystallinity with fewer crystal defects [38]. The high intensity of green emission is attributed to a large number of ionized oxygen deficiencies. The increasing growth time of nanorods increases the kinetic energy of the atoms in ZnO lattice, which in turn increases the evaporation of oxygen atoms than adsorption amount, and hence,

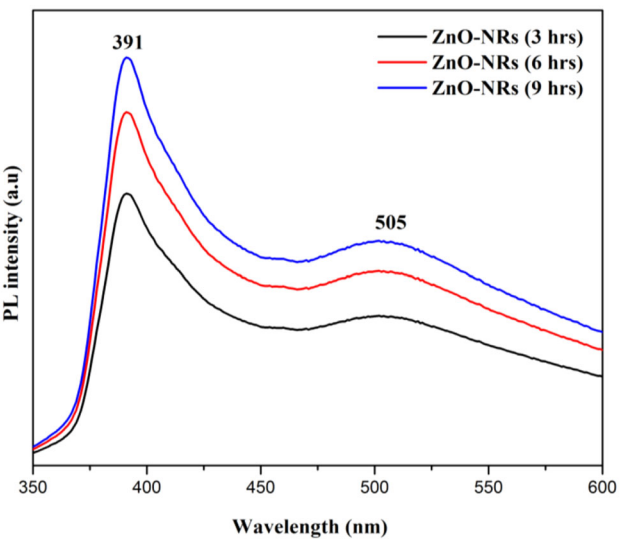

Fig. 9 Photoluminescence spectra of ZnO NRs prepared at various growth times

new vacancies are generated [39]. Figure 10a–d shows the UV–Vis spectra of natural dye extract-absorbed ZnO NRs. The absorption peaks for *hibiscus rosa-sinensis* extract are observed at 535 nm (Fig. 10b). Schematic diagram of *hibiscus rosa-sinensis* dye-sensitized ZnO nanorods are shown in Fig. 10c. The absorption band is broadened and red shifted compared to the UV–Vis spectra of dye solution (Fig. 10d). The broadening of peaks showed the possibility of a larger amount of dye molecules adsorbed on the oxide surface, which in turn increased the cell performance. Moreover, the red shift shows the dye molecules are absorbed onto ZnO NRs surface and this leads to better light-harvesting nature [40].

3.6 Electrical properties

The electrical properties of ZnO NRs are studied using Hall effect measurement at room temperature. The electrical properties can be controlled by adjusting the growth process. Table 1 summarizes the electrical properties of ZnO nanorods grown on ITO substrate with different growth times. The decrease in resistivity of the ZnO NRs with increasing growth time is due to the decrease in the volume of grain boundaries. The recorded lowest resistivity value of 0.75×10^{-4} Ω cm for the nanorods prepared at 9 h is due to the improved film crystallinity. The increase of carrier concentration and mobility with increasing growth time is due to the enhancement of film crystallinity. The enhancement of film crystallinity helps reduce the loss of carriers due to the scattering at the grain boundaries.

3.7 Photovoltaic characterization (*J–V*) of DSSCs

The *J–V* characteristics of DSSCs prepared with ZnO NRs grown on ITO substrates as photoanode at different growth times are shown in Fig. 11a. The DSSCs with ZnO NRs (3 h) showed a short-circuit current density (J_{sc}) of 1 mA/cm^2, open-circuit voltage (V_{oc}) of 0.5 V, and fill factor (FF) 0.54 in the PCE of 0.27%. The J_{sc}, V_{oc}, FF, and PCE of the DSSCs with ZnO NRs prepared at 6 h is 0.55 V, 0.61, 1.78 mA/cm^2, and 0.59% respectively. When the growth time is increased to 9 h, the J_{sc}, V_{oc}, FF, and PCE values are significantly increased and reach a maximum value of 2.25 mA/cm^2, 0.60 V, 0.63, and 0.85% respectively.

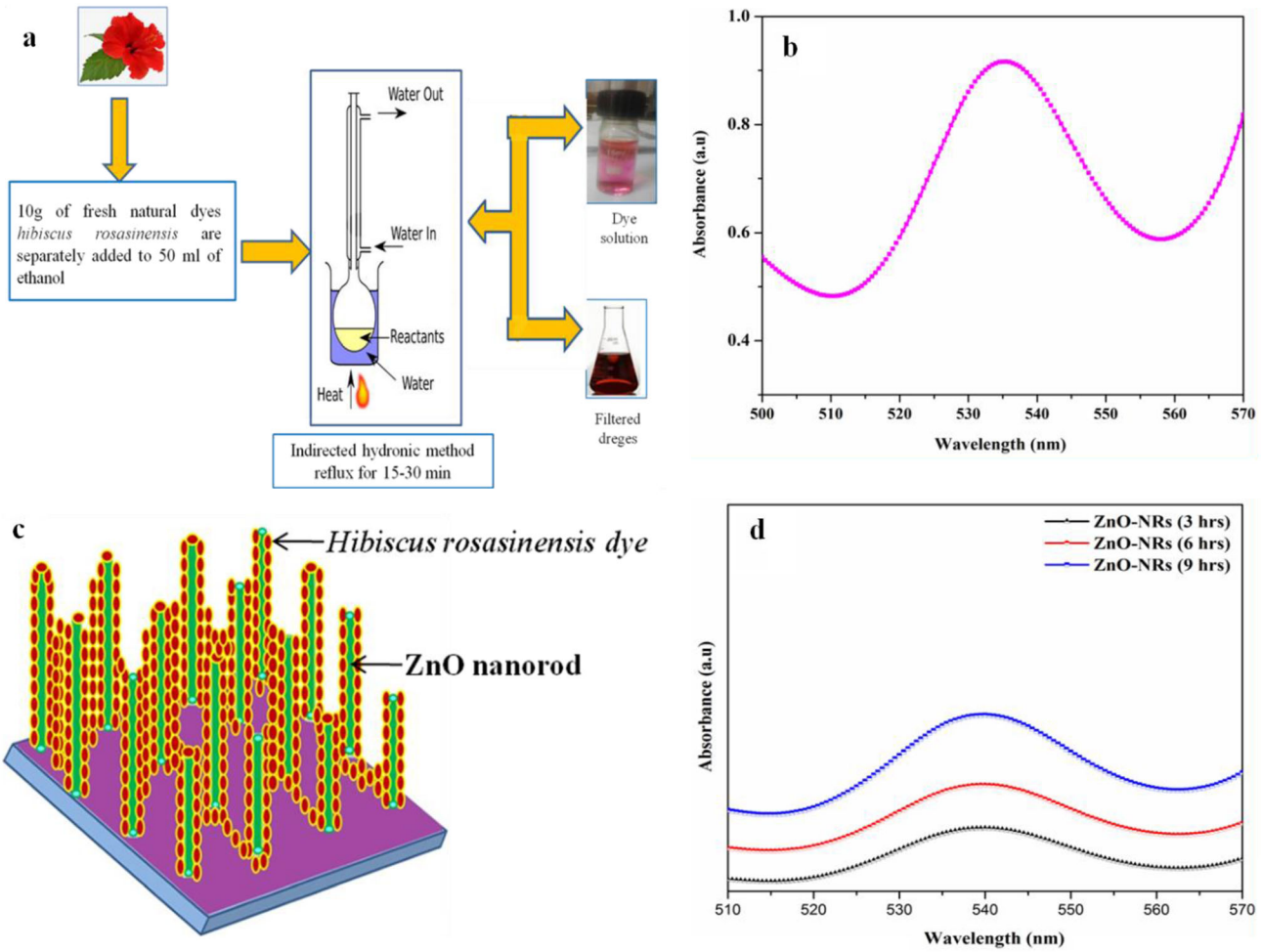

Fig. 10 **a** Dye extract preparation, **b** UV–Vis Spectra of *hibiscus rosa-sinensis* dye extract, **c** Schematic diagram of *hibiscus rosa-sinensis* dye-sensitized ZnO nanorods, **d** UV–Vis Spectra of dye-sensitized ZnO NRs

This result indicates that the *hibiscus rosa-sinensis* dye extract absorbed onto the ZnO NRs surface, absorbs more photons, and helps transfer electron across the dye/ZnO interface. The enhanced device performance with increased growth time is mainly due to the increased J_{sc}, and the higher surface area of ZnO NRs with larger dye loading. Figure 11b shows that the V_{oc} values are increased from 0.5 to 0.6 V, because of the increase of the ZnO quasi-Fermi level with an increasing amount of electron injected from the dye into the conduction band (ZnO). The resistance of the cell, which is offered by ITO substrate, photoanode, electrolyte, and the counter electrode, determines the fill factor of DSSCs. From Fig. 11c, it is clear that the FF value increases along with growth time [40]. In the present study, the power conversion efficiency of 0.85% is obtained for DSSCs with ZnO NRs (9 h) as photoanode and *hibiscus rosa-sinensis* dye extracts as a sensitizer.

The *J–V* characteristics of DSSCs with ZnO NRs as photoanodes and sensitized with *hibiscus rosa-sinensis* natural dye using different solvents are shown in Fig. 12. The intensity of the dye and absorption wavelength also influences the performance and stability of the DSSCs [41]. It is evident from Fig. 12 that *hibiscus rosa-sinensis* dye extracted using ethanol solvent-based DSSCs achieves a maximum η of 0.85% compared to other solvents. The η value of DSSCs using ethanol as solvent is more efficient than that of using water (0.15%) and methanol (0.35%) as solvents. The aggregation of dye molecules is less when anthocyanin is more soluble in ethanol; however, aggregation of dye molecule is more when water is used as solvent. The improved efficiency of DSSCs

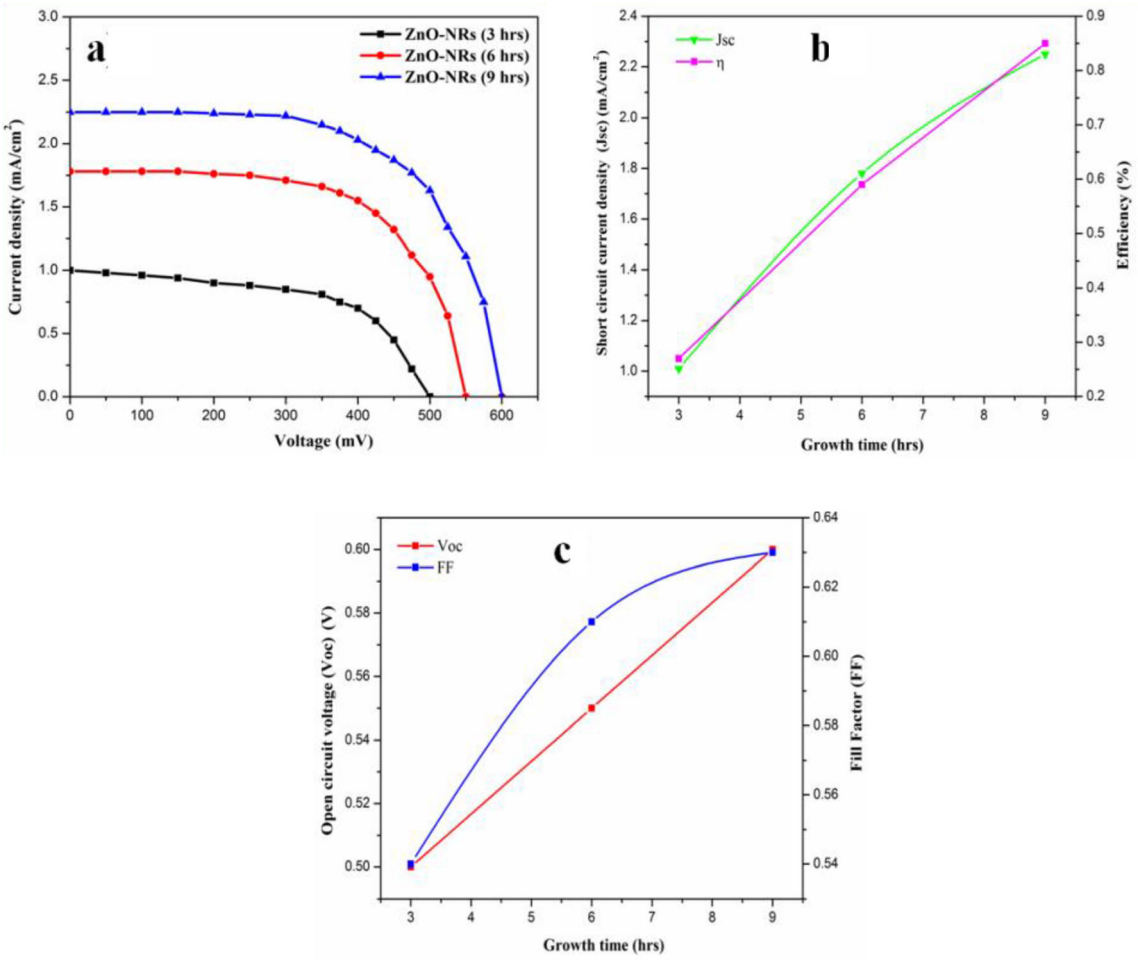

Fig. 11 **a** *J–V* characteristics of ZnO NRs based DSSCs, **b** J_{sc} and η, **c** V_{oc} and FF

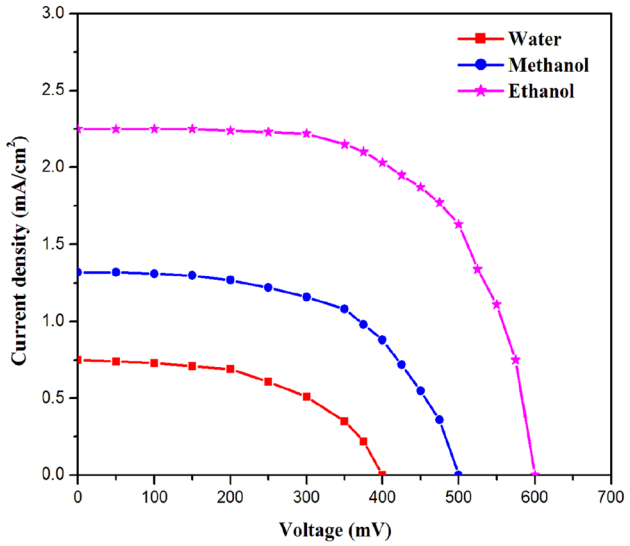

Fig. 12 *J–V* characteristics of DSSCs using *hibiscus* dye with different solvents

might also be due to the uniform and better dispersion of dye molecules on the oxide surface [42].

4 Conclusion

In summary, diameter controlled ZnO NRs were grown on ITO conducting substrates by two steps: (i) seed layer by spray pyrolysis followed by (ii) growth of nanorod using a hydrothermal method at different growth times. The XRD analysis confirmed the wurtzite structure with preferential orientation along (002) direction. FESEM images revealed the uniform distribution of ZnO NRs with hexagonal structure. The presence of Zn and O was confirmed by compositional analysis. A strong near band edge emission (385 nm) and green emission (505 nm) observed from PL spectra confirmed the better crystalline quality with lesser defects. UV–Vis analysis

revealed that the broad absorption band of natural dye extract indicates the absorption of dye molecules onto the ZnO NRs. The maximum PCE of 0.85% was achieved for fabricated DSSCs based on ZnO NRs using growth time at 9 h. The efficiency of DSSCs could also be improved by changing the dye extracting solvents.

References

1. S. Kannan, N.P. Subiramaniyam, S.U. Lavanisadevi, Controllable synthesis of ZnO nanorods at different temperatures for enhancement of dye-sensitized solar cell performance. Mater. Lett. **274**, 127994–127995 (2020)
2. B. O'Regan, M. Grätzel, A low-cost, high-efficiency solar cell based on dye-sensitized colloidal TiO_2 films. Nature **353**, 737–740 (1991)
3. J.B. Baxter, Commercialization of dye sensitized solar cells: present status and future research needs to improve efficiency, stability, and manufacturing. J. Vac. Sci. Technol. A. **30**, 30020801 (2012)
4. J. Gong, J. Liang, K. Sumathy, Review on dye-sensitized solar cells (DSSCs): Fundamental concepts and novel materials. Renew. Sust. Energ. Rev. **16**, 8584–8586 (2012)
5. T.W. Hamann, R.A. Jensen, A.B.F. Martinson, H.V. Ryswyk, J.T. Hupp, Advancing beyond current generation dye-sensitized solar cells. Energy Environ. Sci. **1**, 6678 (2008)
6. A. Saranya, T. Devasena, H. Sivaram, R. Jayavel, Role of hexamine in ZnO morphologies at different growth temperature with potential application in dye sensitized solar cell. Mater. Sci. Semicond. Process. **92**, 108–115 (2019)
7. M. Suchea, S. Christoulakis, K. Moschovis, N. Katsarakis, G. Kiriakidis, ZnO transparent thin films for gas sensor applications. Thin Solid Films **515**, 551–554 (2006)
8. D.-K. Hwang, Oh. Min-Suk, J.-H. Lim, S.-J. Park, ZnO thin films and light-emitting diodes. J. Phys D: Appl. Phys. **40**(22), R387 (2007)
9. C.-L. Kuo, C.-L. Wang, H.-H. Ko, W.-S. Hwang, K.M. Chang, W.-L. Li, H.-H. Huang, Y.-H. Chang, M.-C. Wang, Synthesis of zinc oxide nanocrystalline powders for cosmetic applications. Ceram. Int. **36**, 693–698 (2010)
10. A. Di Mauro, M. ElenaFragalà, V. Privitera, G. Impellizzeri, ZnO for application in photocatalysis: from thin films to nanostructures. Mater. Sci. Semicond. Process. **69**, 44–51 (2017)
11. V.P. Dinesh, R. Sriram kumar, A. Sukhananazerin, J. Mary Sneha, P. Manoj Kumar, P. Biji, Novel stainless steel based, eco-friendly dye-sensitized solar cells using electrospun porous ZnO nanofibers. Nano-Struct. Nano-Objects **19**, 100311 (2019)
12. C.L. Hsu, K.C. Chen, Improving piezoelectric nanogenerator comprises of ZnO nanowires by bending the flexible PET substrate at low vibration frequency. J. Phys. Chem. C **116**, 9351–9355 (2012)
13. P.I. Reyes, C.-J. Ku, Z. Duan, Y. Lu, A. Solanki, K.-B. Lee, ZnO thin film transistor immunosensor with high sensitivity and selectivity. Appl. Phys. Lett. **98**, 173702 (2011)
14. S. Sharma, S. Vyas, C. Periasamy, P. Chakrabarti, Structural and optical characterization of ZnO thin films for optoelectronic device applications by RF sputtering technique. Superlattices Microst. **75**, 378–389 (2014)
15. S.B. Zhu, L.M. Shan, X. Tian, X.Y. Zheng, D. Sun, X.B. Liu, L. Wang, Z.W. Zhou, Hydrothermal synthesis of oriented ZnO nanorod–nanosheets hierarchical architecture on zinc foil as flexible photoanodes for dye-sensitized solar cells. Ceram. Int. **40**, 11663–11670 (2014)
16. P. Sanjay, K. Deep, J. Madhavan, S. Senthil, Natural dyes extracted from fruits of *Phyllanthus reticulatus* as sensitizers in ZnO nanorods based dye sensitized solar cells. Mater. Today Proc. **8**, 284–293 (2019)
17. X. Fang, Y. Li, S. Zhang, Li. Bai, N. Yuan, J. Ding, The dye adsorption optimization of ZnO nanorod-based dye-sensitized solar cells. Sol. Energy **105**, 14–19 (2014)
18. E. Galoppini, J. Rochford, H. Chen, G. Saraf, Y. Lu, A. Hagfeldt, G. Boschloo, Fast electron transport in metal organic vapor deposition grown dye-sensitized ZnO nanorod solar cells. Phys. Chem. B. **110**, 16159–16161 (2006)
19. J.J. Wu, S.C. Liu, Low temperature growth of well-aligned ZnO nanorods by chemical vapor deposition. Adv. Mat. **14**, 215–218 (2002)
20. D.N. Montenegro, A. Souissi, C. Martínez-Tomás, V. Muñoz-Sanjosé, V. Sallet, Morphology transitions in ZnO nanorods grown by MOCVD. J. Cryst. Growth **359**(15), 122–128 (2012)
21. Y.S. Gareth, M. Fuge Michael, N.R. Ashfold, Growth of aligned ZnO nanorod arrays by catalyst-free pulsed laser deposition methods. Chem. Phys. Lett. **396**, 21–26 (2004)
22. Y. Tao, Fu. Ming, A. Zhao, D. He, Y. Wang, The effect of seed layer on morphology of ZnO nanorod arrays grown by hydrothermal method. J. Alloys Compd. **489**, 99–102 (2010)
23. K.M.K. Srivatsa, D. Chhikara, M. SenthilKumar, Synthesis of aligned ZnO nanorod array on silicon and sapphire substrates by thermal evaporation technique. J. Mater. Sci. Technol. **27**(8), 701–706 (2011)
24. S. Baruah, J. Dutta, Effect of seeded substrates on hydrothermally grown ZnO nanorods. J. Sol–Gel Sci. Technol. **50**, 456–464 (2009)

25. N.S. Ridhuan, Y.P. Fong, Z. Lockman, K.A. Razak, Formation of ZnO nanorods via seeded growth hydrothermal reaction. Appl. Mech. Mater. **83**, 116–122 (2011)
26. X. Zhao, J.Y. Lee, C.-R. Kim, J. Heo, C.M. Shin, J.-Y. Leem, H. Ryu, J.-H. Chang, H.C. Lee, W.-G. Jung, C.-S. Son, B.C. Shin, W.-J. Lee, S.T. Tan, J. Zhao, X. Sun, Dependence of the properties of hydrothermally grown ZnO on precursor concentration. Phys. E **41**, 1423–1426 (2009)
27. Q. Li, J. Bian, J. Sun, J. Wang, Y. Luo, K. Sun, Yu. Dongqi, Controllable growth of well aligned ZnO nanorod arrays by low-temperature wet chemical bath deposition method. Appl. Surf. Sci. **256**, 1698–1702 (2010)
28. M. Guo, P. Diao, S. Cai, Hydrothermal growth of well-aligned ZnO nanorod arrays: Dependence of morphology and alignment ordering upon preparing conditions. J. Solid State Chem. **178**, 1864–1873 (2005)
29. J. Rodríguez, F. Paraguay-Delgado, A. López, J. Alarcón, W. Estrad, Synthesis and characterization of ZnO nanorod films for photocatalytic disinfection of contaminated water. Thin Solid Films **519**(2), 729–735 (2010)
30. G. Kenanakis, N. Katsarakis, E. Koudoumas, Influence of precursor type, deposition time and doping concentration on the morphological, electrical and optical properties of ZnO and ZnO: Al thin films grown by ultrasonic spray pyrolysis. Thin Solid Films **555**, 62–67 (2014)
31. Y. Dou, Wu. Fang, C. Mao, L. Fang, S. Guo, M. Zhou, Enhanced photovoltaic performance of ZnO nanorod-based Dye-Sensitized Solar Cells by using Ga doped ZnO seed layer. J. Alloys Compd **633**(5), 408–414 (2015)
32. P. Dhamodharan, C. Manoharan, S. Dhanapandian, P. Venkatachalam, Dye-sensitized solar cell using sprayed ZnO nanocrystalline thin films on ITO as photoanode. Spectrochim. Acta Part A Mol. Biomol. Spectrosc. **136**, 1671–1678 (2015)
33. P. Sanjaya, K. Deepab, J. Madhavanb, S. Senthil, Optical, spectral and photovoltaic characterization of natural dyes extracted from leaves of *Peltophorum pterocarpum* and *Acalypha amentacea* used as sensitizers for ZnO based dye sensitized solar cells. Opt. Mater. **83**, 192–199 (2018)
34. S. Kahraman, F. Bayansal, H.A. Çetinkara, H.M. Çakmak, H.S. Güder, Characterization of CBD grown ZnO films with high c-axis orientation. Mater. Chem. Phys. **134**, 1036–1041 (2012)
35. U. Chaitra, D. Kekuda, K. Mohan Rao, Effect of annealing temperature on the evolution of structural, microstructural, and optical properties of spin coated ZnO thin films. Ceram. Int. **43**, 7115–7122 (2017)
36. Y.-M. Lee, H.-W. Yang, Optimization of processing parameters on the controlled growth of ZnO nanorod arrays for the performance improvement of solid-state dye sensitized solar cells. J. Solid State Chem. **184**, 615–623 (2011)
37. N.S. Ridhuan, K.A. Razak, Z. Lockman, A.A. Aziz, Structural and morphology of ZnO nanorods synthesized using ZnO seeded growth hydrothermal method and its properties as UV sensing. Plos one **7**, e50405-15 (2012)
38. R. Mariappan, V. Ponnuswamy, P. Suresh, Effect of doping concentration on the structural and optical properties of pure and tin doped zinc oxide thin films by nebulizer spray pyrolysis (NSP) technique. Superlattices Microstruct. **52**, 500–513 (2012)
39. X.Q. Meng, D.Z. Shen, J.Y. Zhang, D.X. Zhao, Y.M. Lu, L. Dong, Z.Z. Zhang, Y.C. Liu, X.W. Fan, The structural and optical properties of ZnO nanorod arrays. Solid State Commun. **135**, 179–182 (2005)
40. M. Thambidurai, N. Muthukumarasamy, D. Velauthapillai, C. Lee, *Rosa centifolia* sensitized ZnO nanorods for photoelectrochemical solar cell applications. Sol. Energy **106**, 143–150 (2014)
41. B. Lapornik, M. Prošek, A. Golc Wondra, Comparison of extracts prepared from plant by-products using different solvents and extraction time. J. Food Eng. **71**, 214–222 (2005)
42. K. Wongcharee, V. Meeyoo, S. Chavadej, Dye-sensitized solar cell using natural dyes extracted from rosella and blue pea flowers. Sol. Energy Mater. Sol. Cells. **91**, 566–571 (2007)